A Two-Wave Scheme for Orographic Gravity Wave Drag Parameterization*

WANG Yuan[1,2†](王 元), CAI Ninghao[1](蔡宁浩), and TANG Jinyun[1](唐锦赟)

1 *Department of Atmosphere Sciences, Key Laboratory of Mesoscale Severe Weather/MOE, Nanjing University, Nanjing* 210093

2 *State Key Laboratory of Severe Weather, Chinese Academy of Meteorological Sciences, Beijing* 100081

(Received April 15, 2008)

ABSTRACT

When the magnitude of sub-scale ographic forcing is comparable with explicitly ordinary dynamic forcing, the drag effect reduced by ographic gravity wave is to be significant for maintaining dynamic balance of atmospheric circulation, as well as the momentum and energy transport. Such sub-scale ographic forcing should be introduced into numerically atmospheric model by means of drag being parameterized. Furthermore, the currently mature ographic gravity wave drag (OGWD) parameterization, i.e., the so-called first-generation (based on lineal single-wave theoretical framework) or the second-generation drag parameterization (including an important extra forcing by the contribution of critical level absorption), cannot correctly and effectly describe the vertical profile of wave stress under the influence of ambient wind shearing. Based on aforementioned consideration, a new two-wave scheme was proposed to parameterize the ographic gravity wave drag by means of freely propagating gravity waves. It starts with a second order WKB approximation, and treats the wave stress attenuations caused by either the selective critical level absorption or the classical critical level absorption explicitly; while in the regions where critical levels are absent, it transports the wave stress vertically by two sinusoidal waves and deposits them and then damps them according to the wave saturation criteria. This scheme is thus used to conduct some sample computations over the Dabie Mountain region of East China, as an example. The results showed that the new two-wave scheme is able to model the vertical distribution of the wave stress more realistically.

Key words: ographic gravity wave drag (OGWD), two-wave parameterization of OGWD, critical-level absorption, WKB approximation

1. Introduction

The essential role of the gravity wave drag (GWD) by unresolved topography in budgeting the momentum and energy of the atmospheric general circulation models has been well appreciated (e.g., Palmer et al., 1986; McFarlane, 1987). In the last decades, researchers made great efforts in designating orographic gravity wave drag (OGWD) parameterization schemes of the first and second generations (see Kim et al., 2003; and references therein), and their implementations in global general circulation models (GCMs) showed that the "westerly bias" and the "cold pole" problem accompanying the insufficient model resolutions of the topography can be well alleviated (McFarlane, 1987; Scinocca and McFarlane, 2000).

In all kinds of OGWD parameterization schemes, the treatment of the GWD by means of freely propagating gravity waves (FPGWs) comprises a very important component. Most of these schemes assume that, in treating the GWD by FPGW, the waves stress will be carried and transported upward unchanged by a single sinusoidal wave according to the Eliassen-Palm theorem (Eliassen and Palm, 1961); but if at a certain level, this single sinusoidal wave meets the wave saturation criteria (Lindzen, 1981), thence the wave breaking is assumed to attenuated the wave stress and the ambient wind is decelerated at that level as a result; furthermore, if a zero wind level (i.e., the classical critical level) is encountered in propagating this single sinusoidal wave, the wave stress is deposited and damped completely and the ambient wind is

*Supported jointly by the State Natural Science Foundation of China under Grant Nos. 40775034, 40575017, and 90715031; the Natural Science Foundation of Jiangsu under Grant No. BK99020; and the open project of State Key Laboratory of Severe Weather, Chinese Academy of Meteorological Sciences.

†Corresponding author: yuanasm@nju.edu.cn.

decelerated there. Even if such single wave OGWD parameterization schemes performed quite well in modeling the vertical distributions of the wave stress (i.e., OGWD), Smith (1980), Hines (1988), Shutts (1995), et al. pointed out that the wave energy (stress) over the topography has a two-branch structure at almost all levels in vertical; Moreover, Shutts (1995, 1998) showed that the selective critical level absorption (this seems always to occur when considering a continuous gravity wave spectrum that launched by the unresolved topography in GCMs is just of such a kind, because each single wave has its own Doppler frequency (DF) and these DFs vanish to zero at different heights, making each single wave filtered out selectively at different levels) will make the wave stress vector misalign with respect to the local ambient wind vector (therefore the assumption usually employed in single wave schemes that the wave stress will always be directed against the ambient wind is violated). Therefore, Scinocca and McFarlane (2000) adopted the suggestion by Hines (1988) and proposed a two-wave scheme to model the vertical distribution of the wave stress. Their numerical tests indicated that such a two-wave scheme did give results more realistic than that by the one-wave scheme (by allowing more wave stress to be deposited into the middle atmosphere, depending on season). However, their two-wave scheme did not treat the selective critical level absorption explicitly, and the angles among the wave stress vectors conveyed by the two single sinusoidal waves and the surface wind vector once being determined (at the surface level) will keep unchanged in propagating the wave stress upward. This just contradicts the discovery in Shutts (1998), where the two-branch structure of the wave energy is found to vary vertically in a directionally sheared ambient flow.

In order to formulate a physically more sound OGWD parameterization scheme, in this paper, a new two-wave scheme that treats explicitly the classical critical level absorption, the selective critical level absorption, and the wave breaking process accompanying the wave saturation was proposed for the GWD by the FPGW. The work is organized as following: Section 2 gives the details in designating the new two-wave scheme; Section 3 gives the results when this new scheme was applied over the Dabie Mountain region; and Section 4 gives the major conclusions and further discussions of the present work.

2. Scheme designation

Perform the 2D Fourier transform to Eqs.(A7)-(A11) in Appendix A, then some cross eliminations lead to

$$\hat{\boldsymbol{U}}_H = \mathrm{i}\frac{(\cos\varphi,\sin\varphi)}{K}\frac{\partial\hat{w}}{\partial z} + \mathrm{i}\frac{\hat{w}(\sin\varphi,-\cos\varphi)}{K} \cdot\frac{U_z\sin\varphi - V_z\cos\varphi}{U_n} - \mathrm{i}\frac{\Gamma_1}{K}(\cos\varphi,\sin\varphi)\hat{w}, \quad (1)$$

where $U_n = U\cos\varphi + V\sin\varphi = U_g\cos(\varphi-\chi)$ is the component of the ambient wind $\boldsymbol{U} \equiv U_g(\cos\chi,\sin\chi)$ when projected into the direction of the wave vector $\boldsymbol{K} \equiv K(\cos\varphi,\sin\varphi)$, and $\mathrm{i} = \sqrt{-1}$ is the imaginary unit.

From Eq.(1) the wave stress per unit area can be expressed as

$$\begin{aligned}\boldsymbol{\tau}_s &= -\frac{1}{XY}\int_{-\infty}^{\infty}\int_{-\infty}^{\infty}\overline{\rho\boldsymbol{U}'_H w'}\mathrm{d}x\mathrm{d}y\\ &= -\frac{\rho_0}{4\pi^2XY}\int_0^{\infty}\int_0^{2\pi}\hat{\boldsymbol{U}}_H\hat{w}^*K\mathrm{d}K\mathrm{d}\varphi\\ &= -\frac{\rho_0}{4\pi^2XY}\int_0^{\infty}\int_0^{2\pi}\mathrm{i}(\cos\varphi,\sin\varphi)\frac{\partial\hat{w}}{\partial z}\hat{w}^*\mathrm{d}K\mathrm{d}\varphi\\ &= -\frac{\rho_0}{4\pi^2XY}\int_0^{\infty}\int_{-\pi/2}^{\pi/2}\mathrm{i}(\cos\varphi,\sin\varphi)(\frac{\partial\hat{w}}{\partial z}\hat{w}^*\\ &\quad -\frac{\partial\hat{w}^*}{\partial z}\hat{w})\mathrm{d}K\mathrm{d}\varphi, \end{aligned} \quad (2)$$

where X, Y are respectively the length and width of the region under consideration and the asterisk is used to designate the complex conjugate.

Define the response function

$$R(K,\varphi) = \mathrm{Re}\Big[\frac{1}{2\mathrm{i}|\hat{w}(K,\varphi,0)|^2}\Big(\frac{\partial\hat{w}}{\partial z}\hat{w}^* - \frac{\partial\hat{w}^*}{\partial z}\hat{w}\Big)\Big], \quad (3)$$

where $\mathrm{Re}(s)$ means taking the real part of a given variable s. Also note, for the ideal flow considered here,

the E-P theorem states that $\mathrm{d}\tau_s/\mathrm{d}z$=0 in regions in absence of critical level absorption and wave saturation, implying that $R(K,\varphi)$ is independent from height in these regions.

Hence when Eq.(3) is entered into Eq.(2), and use the lower boundary condition $\hat{w}(0) = \mathrm{i}\boldsymbol{K}\cdot\boldsymbol{U}\hat{h}(k,l)$, where

$$\hat{h} = \int_{-\infty}^{\infty}\int_{-\infty}^{\infty} h(x,y)\mathrm{e}^{-\mathrm{i}(kx+ly)}\mathrm{d}x\mathrm{d}y \tag{4}$$

is the 2D Fourier transform of the orographic shape function $h(x,y)$, one yields

$$\boldsymbol{\tau}_s = 2\rho_0 U_g^2(0)\int_0^{\infty}\int_{-\pi/2}^{\pi/2}(\cos\varphi,\sin\varphi)\cos^2[\varphi-\chi(0)] \cdot K^2 R(K,\varphi)A(K,\varphi)\mathrm{d}K\mathrm{d}\varphi, \tag{5}$$

where

$$K\cdot A = \frac{K|\hat{h}|^2}{4\pi^2 XY} = A_1(K)A_2(\varphi) = \Big(\frac{K}{K_0}\Big)^{\gamma}\Big[\frac{1}{2\pi}(C_1 + C_2\cos2\varphi + C_3\sin2\varphi)\Big] \tag{6}$$

is the orographic spectrum of exponent form (Shutts, 1995), where K_0 is some constant, set to 1 km^{-1} in the present investigation.

Introduce the normalized orographic covariance in direction x as following

$$\sigma_{xx}^2 = \frac{1}{XY}\int_0^X\int_0^Y\Big(\frac{\partial h}{\partial x}\Big)^2\mathrm{d}x\mathrm{d}y = \int_{-\infty}^{\infty}\int_{-\infty}^{\infty}A(K,\varphi)K^3\cos^2\varphi\mathrm{d}K\mathrm{d}\varphi. \tag{7}$$

When Eq.(7) is integrated explicitly using Eq.(6), one finds

$$\sigma_{xx}^2 = \frac{(C_1 + C_2/2)}{2(\gamma+3)K_0^{\gamma}}(K_{\mathrm{U}}^{\gamma+3} - K_{\mathrm{L}}^{\gamma+3}). \tag{8}$$

On same arguments, one also has

$$\sigma_{xy}^2 = \frac{C_3}{4(\gamma+3)K_0^{\gamma}}(K_{\mathrm{U}}^{\gamma+3} - K_{\mathrm{L}}^{\gamma+3}), \tag{9}$$

$$\sigma_{yy}^2 = \frac{(C_1 - C_2/2)}{2(\gamma+3)K_0^{\gamma}}(K_U^{\gamma+3} - K_L^{\gamma+3}), \tag{10}$$

where $K_{\mathrm{U}} \leqslant 2\pi N(0)/U_g(0)$ and $K_{\mathrm{L}} \geqslant 2\pi f/U_g(0)$ (f is the conventional Coriolis parameter) are two parameters introduced to place upper and lower bounds of the unresolved orographic spectrum considered in a large scale numerical model.

Since the FPGWs are mostly hydrostatic (Smith, 1979), then from Eqs.(B3)–(B5) in Appendix B, one obtains

$$R(K,\varphi) = \frac{N}{U_n}\Big[1 - \frac{\Gamma_1 U_n}{N}\frac{U_{nz}}{N} - \frac{1}{4}\frac{U_n U_{nzz}}{N^2} - \frac{1}{8}\frac{U_{nz}^2}{N^2} - \frac{1}{2}\Big(\frac{\Gamma_1 U_n}{N}\Big)^2\Big(\frac{U_{nz}}{N}\Big)^2\Big] = B\frac{N}{U_n}. \tag{11}$$

Further, by neglecting the much smaller terms multiplied by $(\Gamma_1 U_n/N)^2$, one then yields

$$B \approx 1 - \Big(\frac{\Gamma_1 U_n}{N}\frac{U_{nz}}{N} + \frac{1}{4}\frac{U_n U_{nzz}}{N^2} + \frac{1}{8}\frac{U_{nz}^2}{N^2}\Big). \tag{12}$$

When Eq.(12) is combined with the fact that $R(K,\varphi)$ is height independent in regions in absence of critical level absorption and wave saturation, one has $R = B_0 N(0)/U_n(0)$, where B_0 is B when evaluated at the surface $z = 0$.

2.1 Deposition of the OGWD

Shutts (1995) once pointed out, when the ambient wind alters its direction along with height, that single waves (with their wave vectors) being perpendicular to the ambient wind vector will be filtered out and deposit their wave stress into the background flow, implying, in such circumstances, the vertical divergence of $\boldsymbol{\tau}_{\mathrm{s}}$ is inevitable.

Therefore, for a certain level shown in Fig.1: because the wave components inside the regions circumscribed by line $\Phi_L = \min_{0,z}\{\widetilde{\chi} - \pi/2\}$ and line $\Phi_U = \max_{0,z}\{\widetilde{\chi} - \pi/2\}$ are filtered off by the ambient flow below height z, where

$$\widetilde{\chi} = \begin{cases} \chi & |\chi| \leqslant \pi/2, \\ \chi - \mathrm{sgn}(\chi)\pi & \pi/2 < |\chi| \leqslant \pi, \end{cases} \tag{13}$$

one only needs to consider wave components with their arguments satisfying $\Phi_U \leqslant \varphi \leqslant \Phi_L + \pi$ in computing the wave stress. As a result, one may define

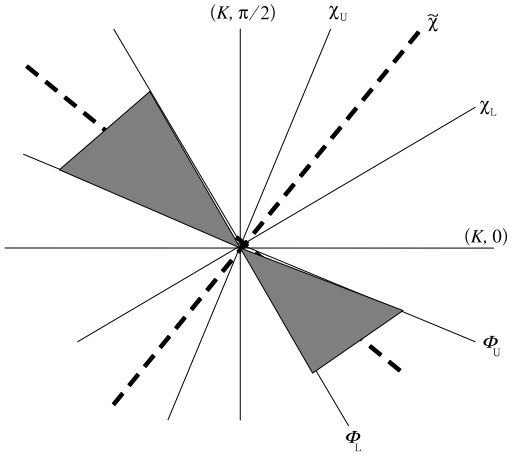

Fig.1. A schematic show of the selective critical level absorption, where $\chi_{\rm U}$ and $\chi_{\rm L}$ are the maximum and minimum arguments that the wind vector had rotated over before reaching level z. This means that the wave components inside the blackened region circumscribed by $\Phi_{\rm U}$ and $\Phi_{\rm L}$ have been filtered off by the ambient flow below level z. This figure is drawn following the Fig.2 in Shutts (1995).

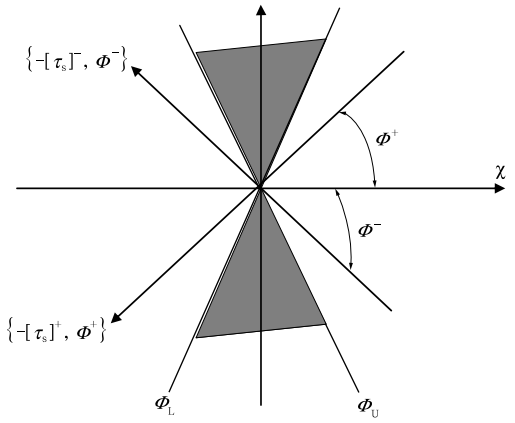

Fig.2. A schematic show for the two-wave approximation at level z, where χ is the wind direction at that level.

$$\boldsymbol{\tau}_s = T\int_{\Phi_{\rm U}}^{\Phi_{\rm L}+\pi}(\cos\varphi,\sin\varphi)B_0\cos(\varphi-\chi(0))A_2(\varphi)\mathrm{d}\varphi$$
$$= T\boldsymbol{E}(\chi(0))\cdot\int_{\Phi_{\rm U}}^{\Phi_{\rm L}+\pi}\boldsymbol{f}(\varphi)\mathrm{d}\varphi, \qquad (14)$$

for the wave stress at level z, where

$$T=\frac{(\gamma+3)K_0^{\gamma}}{K_{\rm U}^{\gamma+3}-K_{\rm L}^{\gamma+3}}\Bigg[\rho_0N(0)U_g(0)\int_{K_{\rm L}}^{K_{\rm U}}K^2\cdot A_1(K)\mathrm{d}K\Bigg]=\rho_0N(0)U_g(0)\Bigg[\frac{\gamma+2}{\gamma+3}\cdot\frac{K_{\rm U}^{\gamma+3}-K_{\rm L}^{\gamma+3}}{K_{\rm U}^{\gamma+2}-K_{\rm L}^{\gamma+2}}\Bigg]^{-1}=\rho_0N(0)U_g(0)\kappa^{-1}. \qquad (15)$$

$\boldsymbol{E}(\chi)$ is defined in Appendix C, and κ is some wavenumber-like parameter (for its determination, readers may refer to Gregory et al. (1998) and Tang (2006)).

Furthermore, if we define

$$[\boldsymbol{\tau}_{\rm s}]^+=T\boldsymbol{E}(\chi(0))\cdot\int_{\Phi_{\rm U}}^{\widetilde{\chi}}\boldsymbol{f}(\varphi)\mathrm{d}\varphi$$
$$[\boldsymbol{\tau}_{\rm s}]^-=T\boldsymbol{E}(\chi(0))\cdot\int_{\widetilde{\chi}}^{\Phi_{\rm L}+\pi}\boldsymbol{f}(\varphi)\mathrm{d}\varphi, \qquad (16)$$

then the wave stress vector $\boldsymbol{\tau}_{\rm s}$ at level z can be resolved into (and thus transported by) two single sinusoidal waves (denoted by wave numbers μ^+ and μ^-), whose strengths are determined by

$$\big|[\boldsymbol{\tau}_{\rm s}]^+\big|=\frac{1}{2}\overline{\rho}(z)(\mu^+)^2N(z)U_g(z)\kappa^{-1}\big|\cos\overline{\Phi}^+\big|(h_m^+)^2$$
$$\big|[\boldsymbol{\tau}_{\rm s}]^-\big|=\frac{1}{2}\overline{\rho}(z)(\mu^-)^2N(z)U_g(z)\kappa^{-1}\big|\cos\overline{\Phi}^-\big|(h_m^-)^2, \qquad (17)$$
$$\Phi^+=\mathrm{atan2}\Big([\tau_{{\rm s}y}]^+,[\tau_{{\rm s}x}]^+\Big),$$
$$\Phi^-=\mathrm{atan2}\Big([\tau_{{\rm s}y}]^-,[\tau_{{\rm s}x}]^-\Big),$$
$$\overline{\Phi}^+=\big|\Phi^+-\chi\big|,\ \overline{\Phi}^-=\big|\Phi^--\chi\big|. \qquad (18)$$

In order to employ the wave saturation criteria, we then compute the non-dimensional amplitudes

$$F^+=\Big|\frac{N(z)h_m^+}{U_g(z)\cos\overline{\Phi}^+}\Big|,\ F^-=\Big|\frac{N(z)h_m^-}{U_g(z)\cos\overline{\Phi}^-}\Big| \qquad (19)$$

for the two single waves defined in Eqs.(16)–(18).

Hence when Eqs.(17)–(19) are evaluated at surface (z=0), and using the constraints

$$F^+=\max\Big(\frac{N(0)h_0}{U_g(0)},F_c\Big),$$
$$F^-=\min\Big(\frac{N(0)h_0}{U_g(0)},F_c\Big), \qquad (20)$$

one obtains

$$\mu^{+}=\Big[\frac{2|[\boldsymbol{\tau}_{\rm s}]^{+}(0)|\kappa}{\rho_0 N(0)U_g(0)\big|\cos\overline{\Phi}^{+}\big|(h_m^{+}(0))^2}\Big]^{1/2}$$
$$\mu^{-}=\Big[\frac{2|[\boldsymbol{\tau}_{\rm s}]^{-}(0)|\kappa}{\rho_0 N(0)U_g(0)\big|\cos\overline{\Phi}^{-}\big|(h_m^{-}(0))^2}\Big]^{1/2} \qquad (21)$$
$$h_m^{+}(0)=\big|\cos\overline{\Phi}^{+}\big|\min\Big(h_0,\frac{F_cU_g(0)}{N(0)}\Big)$$
$$h_m^{-}(0)=\big|\cos\overline{\Phi}^{-}\big|\min\Big(h_0,\frac{F_cU_g(0)}{N(0)}\Big),$$

where h_0 is defined in Eq.(C10) in Appendix C, and F_c is some dimensionless critical height (with a value of 0.4 in the present investigation).

2.2 Computing procedures

Following are the procedures to implement the new two-wave OGWD parameterization scheme:

1) Compute the lunching wave stress vector $\boldsymbol{\tau}_{\rm s}(0)$ with Eq.(14); set $\widetilde{\chi}=\widetilde{\chi}(0)$; $\Phi_{\rm L}=\Phi_{\rm U}=\widetilde{\chi}(0)-\pi/2$ determine $\mu^{+}$and μ^{-} with Eq.(21).

2) Suppose the wave stress vector $\boldsymbol{\tau}_{\rm s}(z_n)$ for the n-th level is ready, thence perform the following procedures at the $(n+1)$-th level.

If $z_{n+1}>z_{\rm top}$, then go to 3); else if $\chi(z_{n+1})=\chi(z_n)+\pi$, then the classical critical level is encountered, set $\boldsymbol{\tau}_{\rm s}(z_{n+1})$=0, go to 3); otherwise perform the following procedures:

① Compute $\widetilde{\chi}(z_{n+1})$, and determine

$$\Phi_{\rm L}=\min\Big\{\Phi_{\rm L}(z_n),\widetilde{\chi}(z_{n+1})-\frac{\pi}{2}\Big\},$$
$$\Phi_{\rm U}=\max\Big\{\Phi_{U}(z_n),\widetilde{\chi}(z_{n+1})-\frac{\pi}{2}\Big\}.$$

② Compute $[\boldsymbol{\tau}_{\rm s}]^{+}$ and $[\boldsymbol{\tau}_{\rm s}]^{-}$ using Eq.(16), and set $T_{\rm ref}$=T and $\boldsymbol{\tau}_{\rm sref}=[\boldsymbol{\tau}_{\rm s}]^{+}+[\boldsymbol{\tau}_{\rm s}]^{-}$.

③ Calculate Φ^{+}, Φ^{-} and $\overline{\Phi}^{+}$, $\overline{\Phi}^{-}$ through Eq. (18).

④ Inverse Eq.(17) and determine h_m^{+} and h_m^{-}.

⑤ Compute F^{+} and F^{-} from Eq.(19), do the functions $F^{+}=\min(F^{+},F_c)$ and $F^{-}=\min(F^{-},F_c)$, inverse Eq.(19) and determine h_m^{+} and h_m^{-}, and then enter the updated h_m^{+} and h_m^{-} into Eq.(17) to obtain the updated $|[\boldsymbol{\tau}_{\rm s}]^{+}|$ and $|[\boldsymbol{\tau}_{\rm s}]^{-}|$, thus one obtains

$$\tau_{{\rm s}x}(z_{n+1})=|[\boldsymbol{\tau}_{\rm s}]^{+}|\cos\Phi^{+}+|[\boldsymbol{\tau}_{\rm s}]^{-}|\cos\Phi^{-},$$
$$\tau_{{\rm s}y}(z_{n+1})=|[\boldsymbol{\tau}_{\rm s}]^{+}|\sin\Phi^{+}+|[\boldsymbol{\tau}_{\rm s}]^{-}|\sin\Phi^{-},$$

the component form for wave stress vector $\boldsymbol{\tau}_{\rm s}(z_{n+1})$, at the same time, one also obtains $T=T_{\rm ref}|\boldsymbol{\tau}_{\rm s}(z_{n+1})|/|\boldsymbol{\tau}_{\rm sref}|$.

⑥Repeat procedure 2).

3) The vertical profile of $\boldsymbol{\tau}_{\rm s}$ is obtained.

3. Results

In this section, we will implement the new two-wave OGWD scheme designated above to compute the wave stress profile over the Dabie Mountain region under different ambient wind profiles.

Tang (2006) found, over the Dabie Mountain region, that the orographic parameters are $\gamma=-1.75, C_1$=2190 m^{2}km, C_2=–373.4 m^2 km, $C_3=-4.3$ m^2 km, and $\kappa=1.30\times10^{-4}$m^{-1}. They will be used to compute $\boldsymbol{\tau}_{\rm s}(z)$ under the following wind profiles, which are

Case 1:

$$U=U_0+\alpha z,\quad V=0, \qquad (22a)$$

Case 2:

$$U=U_0,\quad V=\alpha z, \qquad (22b)$$

and Case 3:

$$U=U_0\cos\beta z,\quad V=U_0\sin\beta z. \qquad (22c)$$

In all the three cases defined in Eq.(22), the buoyancy frequency is set constant, with a value N=0.01 s^{-1}, and the density profile is

$$\overline{\rho}=\rho_0\exp(-z/H), \qquad (23)$$

where ρ_0=1.22 kg m^{-3} and the scale height H=8 km.

Further, we set U_0=10 m s^{-1}, $|\alpha|=\sqrt{10}\times10^{-3}$ s^{-1}, and $|\beta|=\sqrt{10}\times10^{-4}$ m^{-1}, which lead to the Richardson number R_i=10 for the three cases.

3.1 The wave stress profiles

Following the computing procedures listed in Section 2.2, Fig.3 gives the vertical structure of $\boldsymbol{\tau}_{\rm s}$ (i.e., the OGWD) in corresponding to the wind profile given by Eq.(22a). Here, because the wind is backward sheared (i.e., $\alpha<0$) in this computation, it shows that the classical critical level at height $z_c=\sqrt{10}\times10^3$ m prevents any wave action to be leaked upward; furthermore, since there's no wave saturation level between the lower surface and height $z_c=\sqrt{10}\times10^3$ m, the wave stress vector $\boldsymbol{\tau}_{\rm s}$ decreases linearly from the surface to the classical critical level.

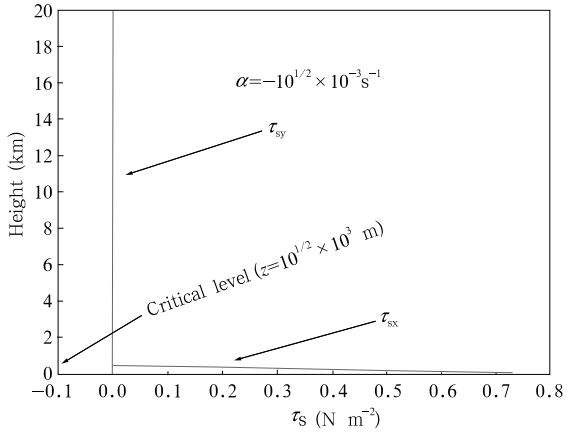

Fig.3. Results for Case 1, only the backward sheared wind is considered, and at the classical critical level $z_c = \sqrt{10} \times 10^3$ m, the wave stress τ_s is completely attenuated.

Corresponding to the wind profiles by Eq.(22b), Fig.4 gives the $\boldsymbol{\tau}_s$ profiles for both the forward sheared wind (i.e., $\alpha > 0$) and the backward sheared wind (i.e., $\alpha < 0$). We found, due to the wind's rotation against height, the wave stress vector $\boldsymbol{\tau}_s$ gradually misaligns with respect to the wind vector, for both the forward and backward sheared winds. For instance, at the level z=20 km (see from the rotating direction of the wind analytical solution for the linearly sheared wind, that the wave stress induced by an isolated circular bell-shaped mountain also varies in the same way as we here found against height. The latter also proves that the new two-wave OGWD scheme presented here is efficient in treating the selective critical level absorption.

Figure 5 gives the vertical structure of $\boldsymbol{\tau}_s$ corresponding to the wind profile by Eq.(22c). Similar to the wind profiles by Eq.(22b), it shows that the OGWD (i.e., the waves stress) is continuously attenuated due to the rotation of the wind vector against

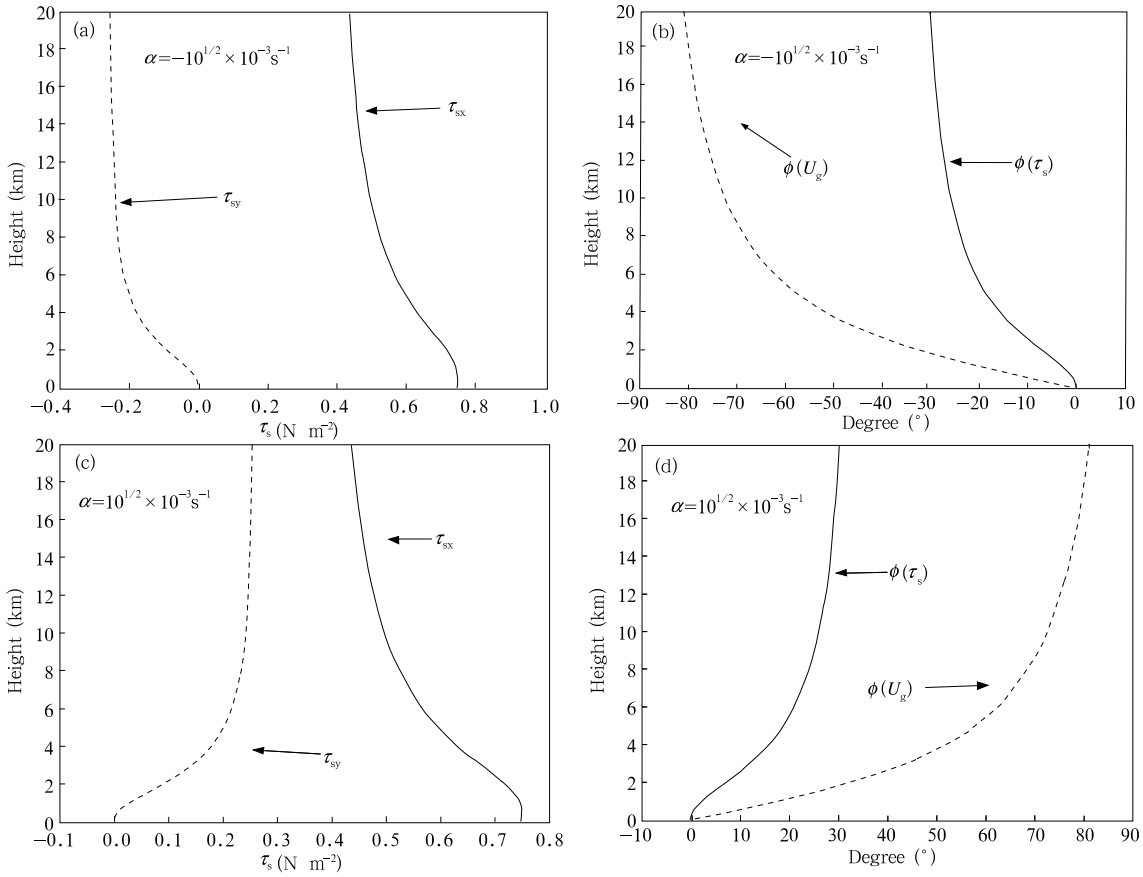

Fig.4. Results for Case 2, (a) and (b) are for backward sheared wind, (c) and (d) are for forward sheared wind. The wave stress vector τ_s always falls behind $\boldsymbol{U}$ (seen from the latter) as the height increases, at z=20 km, the former falls behind the latter about 50°.

the height, and the misalignment between the wind vector and the stress vector is also very significant. However, above the level z=9935 m, no modification to the ambient flow is allowed because the OGWD is completed deposited from below.

As a further example, we then compute the wave stress profile over the Dabie Mountain region when the wind profile is given as a zonal average in winter in middle latitude in the Northern Hemisphere, and the density and the stratification is given by the American Standard Atmosphere 1976. The result is shown in Fig.6, where it is found that there are three attenuation regions by 0–0.5, 20–26.5, and 51.5–80 km. Further analysis reveals that the region by 51.5–80 km is just the location of the westerly in top of the stratosphere. On the other hand, we know the attenuation of the wave stress (i.e., OGWD) rightly means the ambient flow is decelerated there, which means the new two-wave OGWD parameterization scheme is efficient in alleviating the "westerly bias".

4. Conclusion and discussion

Starting with a second order WKB approximation to the Taylor-Goldstein equation, Eq.(B1), a new two-wave scheme to parameterize the OGWD by FPGWs was presented. It was then used to compute the OGWD over the Dabie Mountain region under different ideal wind profiles and a zonal average during winter in middle latitude in the Northern Hemisphere. The results showed that this new two-wave scheme did reveal the misalignment between the wave stress vector and the local ambient wind when the ambient wind alters its direction along with height. Further, the new scheme also proved itself capable of alleviating the

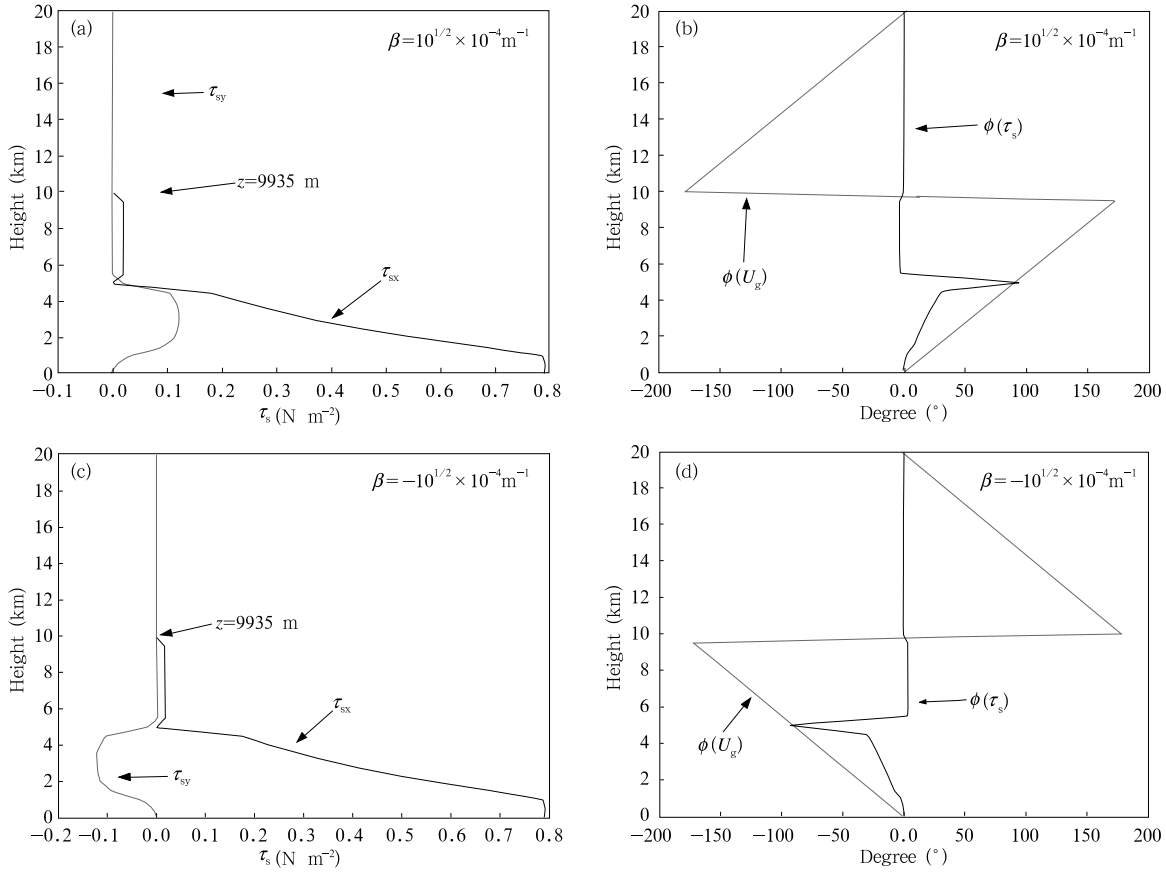

Fig.5. Results for Case 3, under both the counterclockwise ((a) and (b)) and the clockwise rotation ((c) and (d)) of the ambient wind vector along with height, the wave stress vector τ_s vanishes at height z=9935 m, because the ambient wind $\boldsymbol{U}$ has just rotated with half a circle from below and the continuous selective critical levels absorb the waves stress completely.

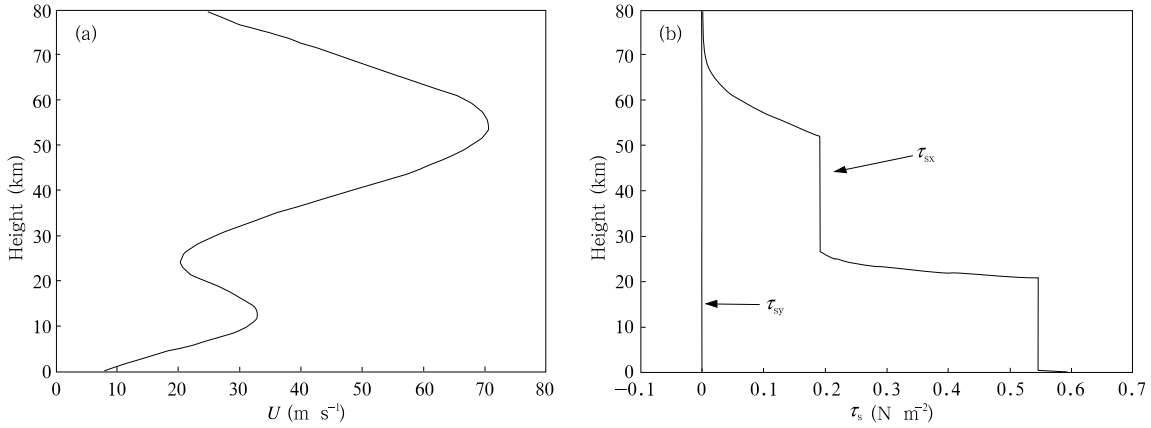

Fig.6. Zonal average wind in winter (a) in middle latitude in the Northern Hemisphere; and the corresponding wave stress profile (b) computed from the wind profile of (a) together with the American Standard Atmosphere 1976.

"westerly bias" by producing wind deceleration in top of the stratosphere where the westerly locates. However, to formulate a complete second generation OGWD parameterization scheme, there is still much work to do, which will be our future efforts.

REFERENCES

Eliassen, A., and E. Palm, 1961: On the transfer of energy in stationary mountain waves. *Geophys. Publ.*, **22**, 1–23.

Gregory, D., G. J. Shutts, and J. R. Mitchell, 1998: A new gravity-wave-drag scheme incorporating anisotropic orography and low-level wave breaking: Impact upon the climate of the UK Meteorological Office Unified Model. *Q. J. R. Meteor.*, **124**, 463–493.

Hines, C. O., 1988: A modelling of atmospheric gravity waves and wave drag generated by isotropic and anisotropic terrain. *J. Atmos. Sci.*, **45**, 309–322.

Kim, Y. J., S. D. Eckermann, and Chun H. Y., 2003: An overview of the past, present and future of gravity-wave drag parameterization for numerical climate and weather prediction models. *Atmos. Ocean*, **41**, 65–98.

Li Jiachun and Zhou Xianchu, 1998: *An Asymptotic Approximation in Mathematic Physics.* Scientific Press, Beijing, 134 pp. (in Chinese)

Lindzen, R. S., 1981: Turbulence and stress owing to gravity wave and tidal breakdown. *J. Geophys. Res.*, **86**, 9709–9714.

McFarlane, N. A., 1987: The effect of orographically excited gravity wave drag on the general circulation of the lower stratosphere and troposphere. *J. Atmos. Sci.*, **44**, 1775–1800.

Palmer, T. N., G. J. Shutts, and R. Swinbank, 1986: Alleviation of a systematic westerly bias in circulation and numerical weather prediction models through an orographic gravity-wave drag parameterization. *Q. J. R. Meteor. Soc.*, **112**, 1001–1039.

Scinocca, J. F., and N. A. McFarlane, 2000: The parameterization of drag induced by stratified flow over anisotropic topography. *Q. J. R. Meteor. Soc.*, **126**, 2353–2393.

Shutts, G. J., 1995: Gravity wave-drag parameterization over complex terrain: The effect of critical-level absorption in directional wind-shear. *Q. J. R. Meteor. Soc.*, **121**, 1005–1021.

Shutts, G. J., 1998: Stationary gravity wave structure in flows with directional wind shear. *Q. J. R. Meteor. Soc.*, **124**, 1421–1442.

Smith, R. B., 1979: The influence of mountains on the atmosphere. *Adv. Geophys.*, **33**, 87–230.

Smith, R. B., 1980: Linear theory of stratified flow past an isolated mountain. *Tellus*, **32**, 348–364.

Tang, J. Y., 2006: A Theoretical Investigation on the Surface Gravity Wave Drag: Its Computation and Parameterization over Complex Terrains. Master-degree dissertation, Nanjing University. (in Chinese)

APPENDIX

A. Governing equations for the perturbations

When the momentum, mass, and thermaldynamic equations for the ideal, steady, fully compressible, non-rotating, and hydrostatic flow are linearized to the first order accuracy, one obtains

$$\boldsymbol{U}\cdot\nabla_H(\boldsymbol{U'}_H)+w'\boldsymbol{U}_z=-\frac{1}{\bar{\rho}}\nabla_H p' \tag{A1}$$

$$\frac{1}{\bar{\rho}}\frac{\partial p'}{\partial z}+\frac{\rho'}{\bar{\rho}}g=0 \tag{A2}$$

$$\boldsymbol{U}\cdot\bigtriangledown_H\Big(\frac{\rho'}{\bar{\rho}}\Big)+\frac{w'}{\bar{\rho}}\frac{\mathrm{d}\bar{\rho}}{\mathrm{d}z}+\nabla_H\cdot\boldsymbol{U'}_H+\frac{\partial w'}{\partial z}=0 \tag{A3}$$

$$\boldsymbol{U}\cdot\bigtriangledown_H\Big(\frac{\theta'}{\bar{\theta}}\Big)+\beta w'=0, \tag{A4}$$

for the perturbations. In above, the primed are the perturbations and the bared are the ambient variables. $\boldsymbol{U'}_H\equiv(u',v')$ is the perturbed horizontal velocity, and $\boldsymbol{U}\equiv(U,V)$ is the horizontal ambient velocity; $\beta=\mathrm{d}(\ln\bar{\theta})/\mathrm{d}z$, $\nabla_H(\cdot)$ is the horizontal gradient operator and others are in their conventional meanings. The subscript z is used to designate partial derivative with respect to variable z.

To close the dynamic system by Eqs.(A1)–(A5), we further introduce

$$-\frac{\rho'}{\bar{\rho}}=\frac{\theta'}{\bar{\theta}}-\frac{1}{\bar{c}_s^2}\frac{p'}{\bar{\rho}}. \tag{A5}$$

Now perform the following transform

$$(\boldsymbol{U}_H,w,\rho,b)=\sqrt{\frac{\bar{\rho}}{\rho_0}}\Big(\boldsymbol{U'}_H,w',\frac{\rho'}{\bar{\rho}},g\frac{\theta'}{\bar{\theta}}\Big)$$
$$\phi=\sqrt{\frac{\rho_0}{\bar{\rho}}}\frac{p'}{\rho_0}, \tag{A6}$$

to Eqs.(A1)–(A5), and employ the small Mach number approximation in the mass equation Eq.(A3) (see Tang (2006) for details), the final version of the governing equations for the perturbations are found as

$$\boldsymbol{U}\cdot\nabla_H(\boldsymbol{U}_H)=-\nabla_H\phi-w\boldsymbol{U}_z \tag{A7}$$

$$\Big(\frac{\partial}{\partial z}+\Gamma_1\Big)\phi-b=0 \tag{A8}$$

$$\Big(\frac{\partial}{\partial z}-\Gamma_1\Big)w=-\nabla_H\cdot\boldsymbol{U}_H \tag{A9}$$

$$\boldsymbol{U}\cdot\nabla_H(b)+N^2w=0 \tag{A10}$$

$$\rho=-\frac{b}{g}+\frac{\phi}{c_s^2}, \tag{A11}$$

where $\rho_0=\bar{\rho}(z=0)$, $\Gamma_1=-\beta-S/2$, $S=\bar{\rho}_z/\bar{\rho}$.

B. The WKB approximation

First perform the 2D Fourier transform to Eqs. (A7) and (A11), then after some cross eliminations, the Taylor-Goldstein equation (Tang, 2006) is obtained

$$\hat{w}_{zz}+\Big(\frac{N^2}{U_n^2}-\Gamma_1^2-2\Gamma_1\frac{U_{nz}}{U_n}-\frac{U_{nzz}}{U_n}\Big)\hat{w}=0. \tag{B1}$$

Under the assumption of the slowly variation of $\boldsymbol{U}$ along with height, a WKB approximation (Li and Zhou, 1998) satisfying the radiation condition at the upper boundary to Eq.(B1) may be found

$$\hat{w}(Z)=\hat{w}(0)\exp\Big\{\mathrm{i}\varepsilon^{-1}\int_0^Z\sum_{j=1}^{\infty}\varepsilon^j m_j(\xi)\mathrm{d}\xi\Big\}, \tag{B2}$$

where $Z=\varepsilon z$, ε is some small parameter, being proportional with $R_i^{-1/2}$, and the zeroth, first, and second order vertical wave-numbers $m_j(j=0,1,2,\cdots)$ are

$$m_0=\frac{N}{U_n} \tag{B3}$$

$$\varepsilon m_1=\frac{N}{U_n}\cdot\Big(-\frac{\Gamma_1U_n}{N}\cdot\frac{U_{nz}}{N}-\frac{\mathrm{i}}{2}\frac{U_{nz}}{N}\Big) \tag{B4}$$

$$\begin{aligned}\varepsilon^2m_2=\frac{N}{U_n}\Big\{\Big[&-\frac{1}{4}\Big(\frac{U_nU_{nzz}}{N^2}+\frac{U_{nz}^2}{2N^2}\Big)\\&-\frac{1}{2}\Big(\frac{\Gamma_1U_n}{N}\Big)^2\cdot\Big(\frac{U_{nz}}{N}\Big)^2\Big]-\mathrm{i}\Big[\frac{\Gamma_1U_n}{2N}\\&\cdot\frac{U_nU_{nzz}}{N^2}+\frac{\Gamma_1U_n}{2N}\cdot\frac{U_{nz}^2}{N^2}\Big]\Big\}.\end{aligned} \tag{B5}$$

C. Some formulas and relevant results used in this work

Definition of $\boldsymbol{E}(\chi)$ (referred in Eq.(14)) and some further relevant results are

$$\begin{aligned}B_0&=\beta_1+\beta_2\cos2\varphi+\beta_3\sin2\varphi\\&=\Big[1-\frac{\Gamma_1(U_0U_{0z}+V_0V_{0z})}{2N^2(0)}-\frac{U_0U_{0zz}+V_0V_{0zz}}{8N^2(0)}\\&\quad-\frac{U_{0z}^2+V_{0z}^2}{16N^2(0)}\Big]-\Big[\frac{\Gamma_1(U_0U_{0z}-V_0V_{0z})}{2N^2(0)}\\&\quad+\frac{U_0U_{0zz}-V_0V_{0zz}}{8N^2(0)}+\frac{U_{0z}^2-V_{0z}^2}{16N^2(0)}\Big]\cos2\varphi\\&\quad-\Big[\frac{\Gamma_1(U_0V_{0z}-V_0U_{0z})}{2N^2(0)}+\frac{U_0V_{0zz}-V_0U_{0zz}}{8N^2(0)}\\&\quad+\frac{U_{0z}V_{0z}}{8N^2(0)}\Big]\sin2\varphi,\end{aligned} \tag{C1}$$

$$
\begin{aligned}
&D_1 = 2C_1\beta_1 + C_2\beta_2 + C_3\beta_3,\\
&D_2 = 2(C_2\beta_1 + C_1\beta_2),\\
&D_3 = 2(C_3\beta_1 + C_1\beta_3),\\
&D_4 = C_2\beta_2 - C_3\beta_3,\\
&D_5 = C_2\beta_3 + C_3\beta_2,
\end{aligned}
\tag{C2}
$$

$$
\begin{aligned}
&E_{1x} = 2D_1 + D_2 + D_3\tan\chi,\\
&E_{2x} = 2(D_1 + D_2) + D_4 + D_5\tan\chi,\\
&E_{3x} = 2D_3 + D_5 + (2D_1 - D_4)\tan\chi,\\
&E_{4x} = 2D_4 + D_2 - D_3\tan\chi,\\
&E_{5x} = 2D_5 + D_3 + D_2\tan\chi,\\
&E_{6x} = D_4 - D_5\tan\chi,\\
&E_{7x} = D_5 + D_4\tan\chi,
\end{aligned}
\tag{C3}
$$

$$
\begin{aligned}
&E_{1y} = 2D_1 - D_2 + D_3\mathrm{ctan}\chi,\\
&E_{2y} = 2(D_2 - D_1) - D_4 + D_5\mathrm{ctan}\chi,\\
&E_{3y} = 2D_3 - D_5 + (2D_1 - D_4)\mathrm{ctan}\chi,\\
&E_{4y} = 2D_4 - D_2 - D_3\mathrm{ctan}\chi,\\
&E_{5y} = 2D_5 - D_3 + D_2\mathrm{ctan}\chi,\\
&E_{6y} = -D_4 - D_5\mathrm{ctan}\chi,\\
&E_{7y} = -D_5 + D_4\mathrm{ctan}\chi,
\end{aligned}
\tag{C4}
$$

$$
\begin{aligned}
&\boldsymbol{E}_x(\chi) = [E_{x1}\ E_{x2}\ E_{x3}\ E_{x4}\ E_{x5}\ E_{x6}\ E_{x7}],\\
&\boldsymbol{E}_y(\chi) = [E_{y1}\ E_{y2}\ E_{y3}\ E_{y4}\ E_{y5}\ E_{y6}\ E_{y7}],\\
&\boldsymbol{E}(\chi) = \frac{K_{\mathrm{U}}^{\gamma+3} - K_{\mathrm{L}}^{\gamma+3}}{8\pi(\gamma+3)K_0^{\gamma}} \left[\begin{array}{c} \boldsymbol{E}_x(\chi)\mathrm{cos}\chi \\ \boldsymbol{E}_y(\chi)\mathrm{sin}\chi \end{array}\right]
\end{aligned}
\tag{C5}
$$

$$
\boldsymbol{f}(\varphi) = [1\ \cos2\varphi\ \sin2\varphi\ \cos4\varphi\ \sin4\varphi\ \cos6\varphi\ \sin6\varphi]^{\mathrm{T}}.
$$

In particular, when the ambient flow is assumed vertically homogenous, the above become

$$
B_0 = \beta_1 = 1, \quad \beta_2 = \beta_3 = 0
$$

$$
\begin{aligned}
&D_1 = 2C_1, \quad D_2 = 2C_2,\\
&D_3 = 2C_3, \quad D_4 = D_5 = 0,
\end{aligned}
\tag{C6}
$$

$$
\begin{aligned}
&E_{1x} = 2D_1 + D_2 + D_3\tan\chi, \quad E_{2x} = 2(D_1 + D_2)\\
&E_{3x} = 2D_3 + 2D_1\tan\chi, \quad E_{4x} = D_2 - D_3\tan\chi,\\
&E_{5x} = D_3 + D_2\tan\chi, \quad E_{6x} = E_{7x} = 0,
\end{aligned}
\tag{C7}
$$

$$
\begin{aligned}
&E_{1y} = 2D_1 - D_2 + D_3\mathrm{ctan}\chi, \quad E_{2y} = 2(D_2 - D_1)\\
&E_{3y} = 2D_3 - 2D_1\mathrm{ctan}\chi, \quad E_{4y} = -D_2 - D_3\mathrm{ctan}\chi\\
&E_{5y} = -D_3 + D_2\mathrm{ctan}\chi, \quad E_{6y} = E_{7y} = 0.
\end{aligned}
\tag{C8}
$$

With Eqs.(C6)–(C7), it is easy to verify

$$
\boldsymbol{\tau}_{\mathrm{s}}(0) = T(0)\kappa^{-1} \left[\begin{array}{c} \sigma_{xx}^2\mathrm{cos}\chi + \sigma_{xy}^2\mathrm{sin}\chi \\ \sigma_{yy}^2\mathrm{sin}\chi + \sigma_{xy}^2\mathrm{cos}\chi \end{array}\right], \tag{C9}
$$

$$
\begin{aligned}
h_0^2 &= \frac{1}{XY}\int_0^X\int_0^Y h^2\mathrm{d}x\mathrm{d}y = \int_{-\infty}^{\infty}\int_{-\infty}^{\infty} A(k,l)\mathrm{d}k\mathrm{d}l\\
&= \int_0^{\infty}\int_0^{2\pi} A(K,\varphi)K\mathrm{d}\varphi\mathrm{d}K.
\end{aligned}
\tag{C10}
$$